GDCh Research Article Angewandte International Edition Chemie www.angewandte.org

How to cite: *Angew. Chem. Int. Ed.* **2024**, *63*, e202410217
doi.org/10.1002/anie.202410217

Host-Guest Systems

Supramolecular Complex of Cucurbit[7]uril with Diketopyrrolopyrole Dye: Fluorescence Boost, Biolabeling and Optical Microscopy

Dojin Kim, Mariano L. Bossi, Vladimir N. Belov,* and Stefan W. Hell*

Dedicated to Prof. Armin de Meijere on the occasion of his 85th birthday

Abstract: New photostable and bright supramolecular complexes based on cucurbit[7]uril (CB7) host and diketopyrrolopyrole (DPP) guest dyes having two positively charged 4-(trimethylammonio)phenyl groups were prepared and characterized. The dye core displays large Stokes shift (in H_2O, abs./emission max. 480/550 nm; ε~19000, $\tau_{fl} > 4$ ns), strong binding with the host (~560 nM K_d) and a linker affording fluorescence detection of bioconjugates with antibody and nanobody. Combination of protein-functionalized DPP dye with CB7 improves photostability and affords up to 12-fold emission gain. Two-color confocal and stimulated emission depletion (STED) microscopy with 595 nm or 655 nm STED depletion lasers shows that the presence of CB7 not only leads to improved brightness and image quality, but also results in DPP becoming cell-permeable.

Introduction

The progress in the chemistry of fluorescent dyes with functional groups often leads to advances in biology-related optical superresolution microscopy, (bio)analytical chemistry and chemistry of materials.[1] A variety of fluorophores including rhodamines, their carbo- and silicon-analogs, cyanines, and coumarins have been developed and widely used in life and material science.[2] Bright and photostable fluorescent dyes are highly demanded as the number of photons emitted from a probe is a key factor for the success of detection and imaging. However, the brightness (product of the extinction coefficient and fluorescence quantum yield) and the photostability of organic dyes are often significantly reduced in aqueous solutions (compared to organic solvents) and even more when bound to a protein of interest. The rather hydrophobic fluorescent dye cores are prone to (self)aggregation (π-stacking of planar fluorophores), and non-specific labeling due to "sticking" of the emitters to lipophilic structures (e.g., cellular membranes). These shortcomings are particularly undesirable in super-resolution microscopy,[3] where spatial resolution down to the molecular scale is expected, since they compromise imaging performance by increasing off-target binding and reducing the signal-to-noise ratio. Therefore, the discovery and development of new fluorophores and alternative strategies to improve the hydrophilicity of the fluorescent markers and reduce the influence of the environment on their properties and performance in optical microscopy are highly desired.

The inherent disadvantages of lipophilic fluorophores can be overcome by decoration of the dye cores with polar groups[2] or by incorporation into the supramolecular complexes[4] The host–guest strategy is particularly attractive because the host not only improves the dye's hydrophilicity and water solubility, but also isolates and protects the guest from the environment.[4] For example, Mohanty and Nau encapsulated a rhodamine dye with cucurbit[7]uril (CB7) to achieve a remarkable increase in photostability.[5] Importantly, the size of complex remains small (<3 nm), on the order of or smaller than most proteins and other biomolecules. Despite several research groups having demonstrated bioimaging applications using supramolecular complexes,[6] the applicability of supramolecular chemistry in modern super-resolution optical microscopy techniques has rarely been explored.[7] For example, different fluorophores containing isopercolic acid residues were encapsulated in cyclodextrins to boost their emission by the suppression of nonradiative relaxation pathways, and successfully imaged lysosomes in HeLa cells with super-resolution STED microscopy.[7a] In another example, a supramolecular assembly of a photochromic diarylethene and CB7 exhibited extremely high photo-fatigue resistance in water (ca. 2500 switching cycles) and afforded super-resolution imaging with low light intensities by RESOLFT microscopy.[7b] One of the main challenges for the application of supramolecular complexes in bioimaging is their instability and dissociation

[*] Dr. D. Kim, Dr. V. N. Belov, Prof. Dr. S. W. Hell
Department of NanoBiophotonics
Max Planck Institute for Multidisciplinary Sciences (MPI-NAT)
Am Fassberg 11, 37077 Göttingen (Germany)
E-mail: vladimir.belov@mpinat.mpg.de
Dr. M. L. Bossi, Prof. Dr. S. W. Hell
Department of Optical Nanoscopy
Max Planck Institute for Medical Research (MPI-MR)
Jahnstrasse 29, 69120 Heidelberg (Germany)
E-mail: Mariano.Bossi@mr.mpg.de

in aqueous media or in cells due to the presence of nucleophiles, proteins and ionic buffers.[7c] These challenges motivated us to search for and synthesize organic dyes capable of supramolecular host–guest interaction, with enhanced performance in confocal and STED microscopy of cells and biological specimen.

Results and Discussion

Our approach involves a newly designed host–guest pair which, upon complexation, shows emission enhancement and improved photostability in fluorescence (super-resolution) microscopy applications. As a guest dye core, we selected a bis-lactam-based DPP (3,6-diaryl-2,5-dihydropyrrolo[3,4-*c*]pyrrole-1,4-dione), known for large brightness and chemical stability of its derivatives.[8] In addition, the DPP core contains multiple positions to which the functional groups may be attached, and this makes DPP a versatile platform for diverse applications. For example, DPP derivatives have been extensively used as inks and pigments (e.g., Pigment Red 254, nicknamed "Ferrari Red", Figure 1),[9] in organic solar cells, in the design of fluorescent sensors for biologically relevant analytes (e.g. ROS, metal cations, cyanide)[9b] and several other optoelectronic applications. As a macrocyclic host molecule, CB7 was chosen because of its high solubility in water (≈5 mM), its favorable size (≈200 Å^3) that can accommodate a large range of small molecules such as drugs and organic fluorophores, and its demonstrated biocompatibility.[4a,c–d]

In the design of our fluorescent marker, we exploited the high binding affinity of CB7 for positively charged residues,[10] to decorate the DPP core at the *para*-phenyl positions with 4-(trimethylammonio)phenyl groups. *N,N′*-Dialkylation of the pyrrole rings is essential to provide solubility in organic solvents, thus facilitating following modifications and the resulting purification process.[8a] We first synthesized model compound 3,6-bis[4′-(trimethylamonio)biphenyl-4-yl]-2,5-dihydropyrrolo[3,4-*c*]pyrrole-1,4-dione (DPP) to test the binding and photophysical properties. In general, 3,6-bis-(biphenyl)diketopyrrolopyrroles with various "outer" phenyl rings are available via Suzuki–Miyaura reaction.[11] We further prepared **DPP-COOH**, containing two carboxylic acids residues attached via C_5-linkers, as well as amino and thiol reactive derivatives intended for bioconjugation (Figure 1). The synthetic details are given in the Supporting Information. The new structures (Figure 1) belonging to the C_{2h} symmetry group are moderately hydrophilic, bear a positive net charge, and hold a potential to have high binding affinity towards CB7. The carboxylic acids residues in **DPP-COOH** are located outside the CB7 binding domains, and are therefore not expected to hinder complexation. To assess the binding property and the complexation ability between guest and host molecules, we performed density functional theory (DFT) calculations (Figures S1, S2). The optimized geometries of host–guest complexes, called **DPP**@CB7 and **DPP-COOH**@CB7, predict a 1:2 complex for both guest dyes, with the diketopyrrolopyrrole cores and the carboxylic acid groups outside the CB7 barrels. The similarity between the structure of both complexes, with the same CB7-CB7 distance (1.6 nm), suggest that the presence of carboxylic acids and their location in **DPP-COOH** should not significantly perturb the complexation.

The photopysical properties of DPP and **DPP**@CB7 were studied in aqueous solutions by means of UV/Vis absorption and photoluminescence (PL) spectroscopy (Figure 2a and Table 1). The positions of absorption and emission maxima of **DPP** agree with the trends reported for numerous diketopyrrolopyrrol derivatives.[10b,11,12] Upon complexation, the absorption maximum of DPP is slightly red-shifted from 475 nm to 481 nm, the absorption increases, and the emission intensity considerably enhanced (Φ_{fl} = 0.62 to 0.81), with the maximum at 550 nm unaffected. The Stokes shifts were found to be large (ca. 2650 cm^{-1}); as for other diketopyrrolopyrroles with electron withdrawing

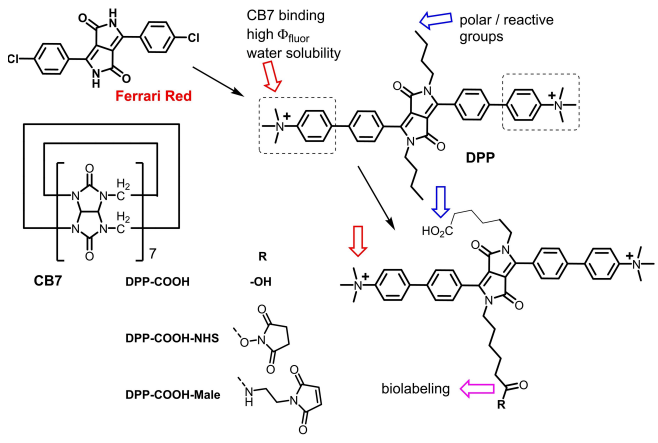

Figure 1. Fluorophore design related to Ferrari Red pigment. The structures of guest molecules prepared in this work—3,6-diaryl-2,5-dihydropyrrolo[3,4-*c*]pyrrole-1,4-diones (**DPP**), **DPP-COOH**; as well as amino and thiol reactive probes (**DPP-COOH-NHS** and **DPP-COOH-Male**, respectively); the host cucurbit[7]uril molecule (CB7).

Table 1: Absorption maxima (λ_{abs}), extinction coefficients (ε), emission maxima (λ_{em}), fluorescence lifetimes (τ_{fl}), fluorescence quantum yields (Φ_{fl}), radiative rate constant (k_r), and nonradiative rate constant (k_{nr}) of DPP and **DPP-COOH**, and their complexes with CB7 (**DPP**@CB7 and **DPP-COOH**@CB7) in water.

	λ_{abs} [nm]	ε×10^{-3} [M^{-1} cm^{-1}]	λ_{emi} [nm]	τ_{fl}[a] [ns]	Φ_{fl}[b] [%]	k_r[c] [10^8 s^{-1}]	k_{nr}[c] [10^8 s^{-1}]
DPP	475	17.9	550	4.80	62	1.29	0.79
DPP@CB7	481	19.6	550	4.57	81	1.77	0.42
DPP-COOH	479	15.8	551	4.78	59	1.23	0.86
DPP-COOH @CB7	481	19.3	551	4.60	77	1.67	0.50

[a] The fluorescence lifetimes were measured at 560 nm and fitted with a mono-exponential decay. [b] The fluorescence quantum yields (absolute values) were measured using an integrating sphere. [c] The radiative and nonradiative rate constants are calculated by $k_r = \Phi_{fl}/\tau_{fl}$ and $\tau_{fl}^{-1} = k_r + k_{nr}$.

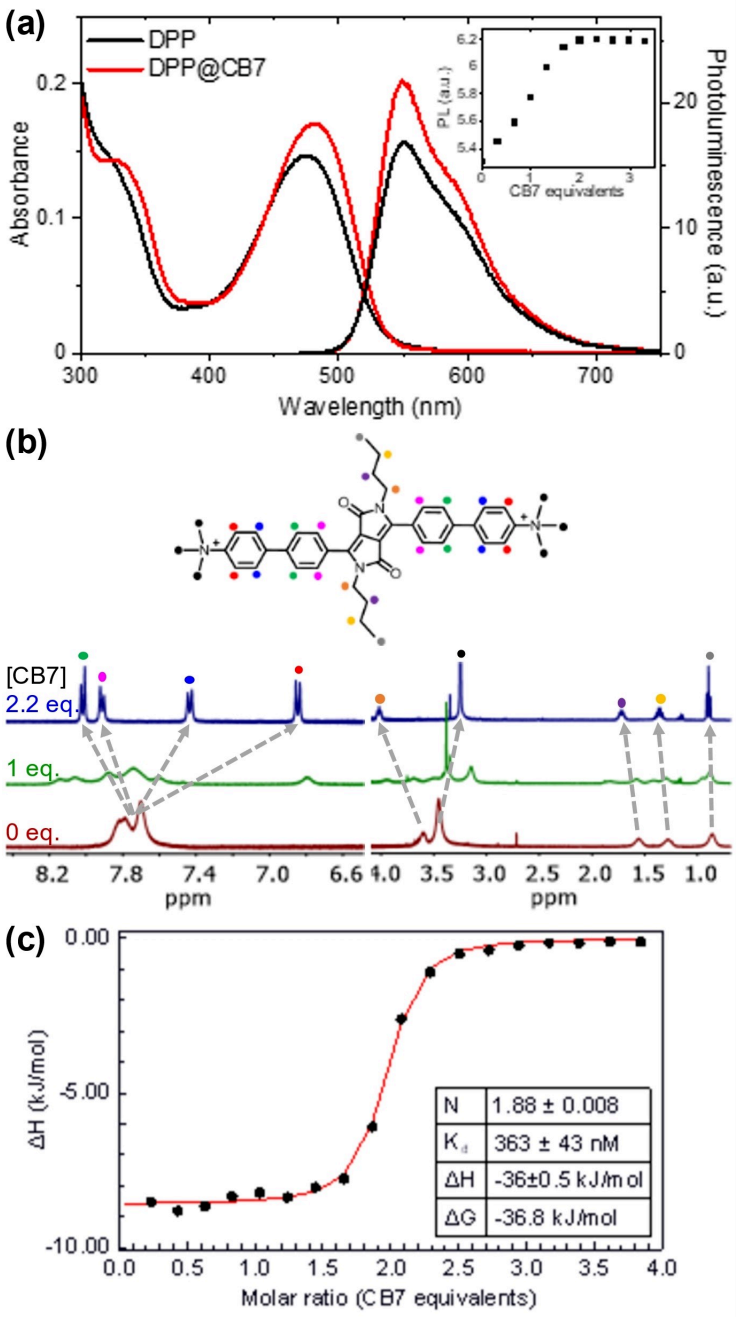

Figure 2. (a) Absorption and photoluminescence (PL, excitation 460 nm) spectra of DPP (black lines) and **DPP**@CB7 complex (red lines) in aqueous solution (10 μM). The inset shows PL changes by varying CB7 amounts. (b) ^{1}H NMR spectra of DPP upon addition of CB7 in D_2O ([DPP] = 2 mM). (c) Isothermal titration calorimetry (ITC) profiles in water at 25 °C: experimental integrated heat (black dots) and fitted curve (red line) of a titration of a 50 μM DPP solution with a 1000 μM CB7 solution.

groups at the terminal positions.[13a] The fluorescence lifetime of DPP slightly decreases upon complexation (τ_{fl} = 4.80 to 4.57 ns) (Figure S3 and Table 1). From the obtained values of τ_{fl} and Φ_{fl}, the radiative and nonradiative rate constants (k_r and k_{nr}) were calculated (Table 1). **DPP**@CB7 has a faster radiative ($k_r = 1.77\times10^8\ s^{-1}$) than nonradiative ($k_{nr} = 0.42\times10^8\ s^{-1}$) pathway, while these two constants show considerably closer values for free DPP ($1.29\times10^8\ s^{-1}$ and $0.79\times10^8\ s^{-1}$, respectively). While a similar tendency has been found for the radiative and non-radiative rates for other dyes, a reduction in the fluorescence lifetime upon encapsulation is rather uncommon: coumarin, xanthene and cyanine dyes were found to have longer fluorescence lifetimes in the host cavity due to lower polarizability in complexes with hosts.[4f,13b] The experimental data on DPP emission (Table 1) agree with the main effect of CB7 binding reducing the rotational freedom of the peripheric phenyl rings,[13a] while the DPP fluorescent core remains

outside of the cavity (Figures S1, S2), as opposed to the case of inherently cationic cores.[4f,13b]

To compare the photostabilities of DPP and **DPP**@CB7, the absorption changes at 480 nm in aqueous solutions were monitored under continuous irradiation with 470 nm light (Figure S4). The **DPP**@CB7 complex was found to be more photostable, as it showed two-times slower bleaching rate than DPP monomer. Next, the complexation behavior was studied by observing the changes in the UV and PL spectra. First, in titration experiments, the absorption and emission intensities changed by adding small portions of CB7 solution to a DPP solution (Figure S5). We observed a gradual increase in DPP emission intensity, until 2 equiv. of CB7 were added and a plateau was reached. The changes in UV and PL spectra at various DPP/CB7 ratios were recorded, and the obtained Job's plots (Figure S6) indicated a 1:2 (DPP:CB7) binding ratio.

To study the complexation in detail, we used ^{1}H NMR spectroscopy and isothermal titration calorimetry (ITC; Figures 2b and 2c). The ^{1}H NMR spectra were recorded in D_2O in the absence of CB7 and with 1 and 2.2 CB7 equivalents. The NMR peaks of DPP without CB7 were rather broad, and all aromatic protons gave one unresolved multiplet at ca. 7.8 ppm. The NMR peaks with one equivalent of CB7 were even broader and shifted, which suggested partial binding. When 2.2 equivalents of CB7 were added, all peaks became sharp and well resolved. The proton multiplets of the "outer" phenyl rings and NMe_3^+ groups (shown as blue, red, and black dots in Figure 2b) were shifted upfield, and those of the "inner" phenyl groups (shown as green and magenta dots) were shifted downfield. These changes indicate that the CB7 hosts interact with the outer phenyl rings, which is in good agreement with the geometry predicted by DFT calculations for **DPP**@CB7. The ITC isotherm of a CB7 solution titrated with a DPP solution (Figure S7) showed a step at 2.5 mol of CB7 per 1 mol of added DPP (N~0.4). In the reversed case, when DPP was titrated with CB7, the sharp transition was observed at the DPP/CB7 molar ratio of 1:2 (corresponding to N~1.9; Figures 2C and S7). Importantly, the dissociation constant (K_d) calculated by this method is ca. 360 nM, which confirms the strong host–guest interaction. These results support that a DPP molecule can be tightly "wrapped" with two CB7 barrels in an aqueous solution.

Next, we investigated the cell permeability of DPP compound and incubated U2OS cells for 30 min with DPP (1 μM) in the cell medium. We observed weakly stained elongated structures concentrated near the nucleus (Figure 3A). Pre-incubation of the dye with CB7 before its addition to the cell medium clearly increases the signal

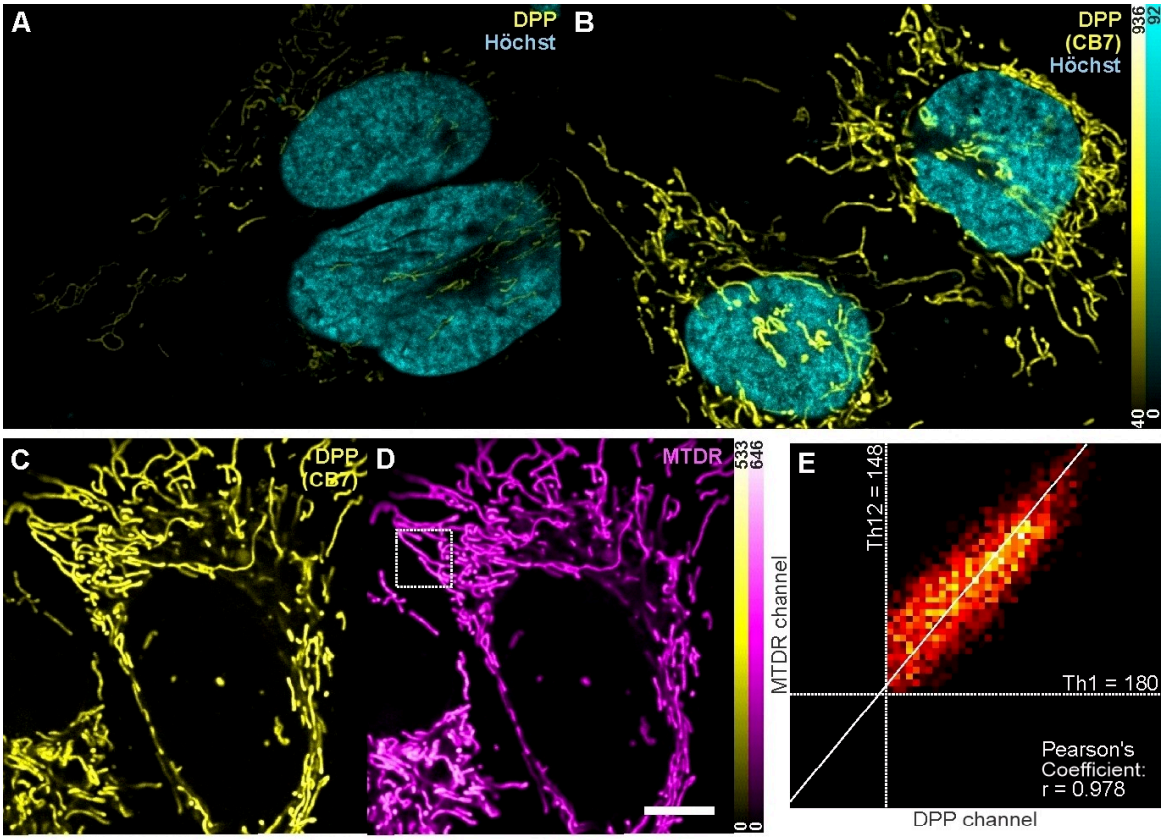

Figure 3. Confocal images of live U2OS cells. Cells were co-labelled with nuclear stain Höchst dye and 1 μM **DPP** without CB7 (A) and **DPP** pre-mixed with CB7 1 mM (B). (C, D) Cells were simultaneously stained with pre-mixed 1 μM **DPP**+CB7 1 mM and MitoTracker Deep Red FM; (E) Corresponding colocalization 2D histogram. Scale bar: 10 μm.

(Figure 3B), suggesting an enhanced cell permeability of the supramolecular complex with respect to the free dye and in agreement with previous reports.[4c,6d,14] As lipophilic cations are known to specifically target mitochondria, we co-stained the cells with commercially available mitochondria marker MitoTracker Deep Red FM. A high colocalization degree (Figure 3C–D) with a Pearson's correlation coefficient value of 0.978 (Figure 3E), confirms the selective targeting of mitochondria with **DPP**@CB7.

To diversify the applicability of this dye through specific labelling, carboxylic acid residues were appended to the side chains in **DPP-COOH** (Figure 1). We first verified that the photophysical properties of **DPP-COOH** and its complex with CB7 (**DPP-COOH**@CB7) were similar. Indeed, only minor differences were found (Table 1 and Figure S8). Beyond that, the complexation behavior of **DPP-COOH** with CB7 was very similar to that of its DPP counterpart (Figures S9, S10).

Then we transformed **DPP-COOH** to amino-reactive *N*-hydroxysuccinimidyl ester **DPP-COOH-NHS** and thiol-reactive maleimide **DPP-COOH-Male** (Figure 1). The former was used for the labeling of antibodies, and the latter for labelling nanobodies incorporating two cysteine residues at the N- and C-terminus. Importantly, only one carboxylic acid group can be activated, while the other one increased the dye polarity. This carboxylate may be (partially) deprotonated. Thus, in their protein adducts, the markers are either double-positively charged, or (at physiological pH) exist in a zwitterionic form with a single positive net charge, reducing dye-aggregation and unspecific labeling of lipophilic structures.

Figures 4A and 4B represent the confocal images of cells stained with primary antibody against tubulin and the secondary antibody labeled with **DPP-COOH-NHS** before and after CB7 addition, respectively. Remarkably, upon CB7 addition, the fluorescence intensity strongly increased (~12-fold; see also Figure S11A–D). This effect was much higher than an increase expected from ensemble experiments (less than 1.3-fold in a cuvette; see Figure 2a and Table 1). These results suggest that the dye emission is highly quenched prior to complexation, possibly due to self-aggregation in the imaging conditions and the close proximity to proteins. Therefore, the observed large fluorescence enhancement might be due to synergistic effects: disaggregation followed by emission enhancement due to host–guest complexation. The aggregation may be aggravated by the salt content in the mounted media used for cells (PBS) and the relatively high degree of labeling (DOL = 5.5). To minimize this problem, we quantitatively labelled nanobodies containing two cysteine residues (Figure S12A). This ensures uniform labelling positions for all proteins, a fixed and defined DOL of 2, and a dye-dye distance of ca. 4 nm.[15] This approach prevents dye-dye aggregation on one and the same nanobody. Confocal images of cells stained with these nanobodies before and after CB7 addition are given in Figures 4C and 4D, displaying a large fluorescence enhancement (> 7 times, Figures 4E–G). These results suggest that despite the loss of signal due to self-aggregation of the dye residues—a known effect for labelled antibodies[16]

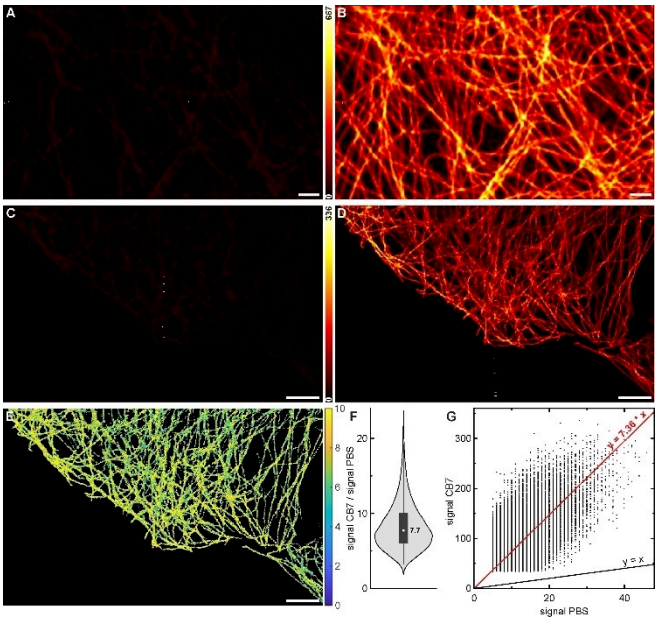

Figure 4. Confocal images of U2OS cells stained with a primary antibody against tubulin and a secondary antibody (A–B) or a secondary nanobody (C–D) labeled with **DPP-COOH-NHS** or **DPP-COOH-Male**, respectively. Images in PBS (A, C) and after the addition of CB7 (B, D). Images are displayed in the same scale (images in PBS scaled to the full range are shown in Figure S11). The ratio of the signal for all pixels (above thresholds) was calculated for D and C and displayed in (E), together with the corresponding violin plot (F) and the signal correlation (G) with a linear fit. The median and the mean of the distribution are 7.71 and 8.35 respectively. Scale bars: 5 μm.

and even nanobodies[17]—the predominant quenching is due to binding with the primary antibody. Assuming that quenching may be produced by proteins, we studied the effect of selected amino-acids reducing the emission of **DPP** (Figure S13).[18] To observe and compare the quenching effects, all amino acids were applied in 0–3 mM concentration range. We found that **DPP** (1.6 μM) is not influenced by histidine, moderately quenched by lysin, methionine and phenylalanine, and strongly by tryptophan. In the latter case, while both static and dynamic quenching mechanisms were observed, the static one is more prominent suggesting that the π–π stacking with tryptophan residues is the main factor responsible for **DPP** quenching. We also confirmed that CB7 (0.8 mM) mitigates the effect in all cases, except for phenylalanine. This amino acid is known to bind CB7 (K_d = 8.7 μM)[19] with lower affinity than DPP does (0.36 μM, Figure 2C). In the presence of CB7, phenylalanine quenched the DPP emission stronger than without CB7 (Figure S13). This may be explained if we assume that the phenylalanine displaces DPP from the complex, thus reducing DPP emission present in the free form (see Figure 2A). Notably, the quenching of phenylalanine in proteins was observed mostly for terminal residues.[20]

The complexation with CB7 in cellular environments also results in a remarkable protection of the dye from undesirable quenching in imaging experiments (Figure 3). Fluorescence-lifetime imaging microscopy (FLIM) indicates

that both static and dynamic quenching mechanisms are operative, since a change in the emission lifetime was observed upon CB7 binding (Figure S14A–B), in addition to the signal amplitude changes. The difference between the signal ratio and the fluorescence lifetime ratio (in the presence and absence of CB7) suggests that static quenching is the main mechanism. For a fairer comparison, we also tested the effects of CB7 addition to the free nanobody (labeled with **DPP-COOH-Male**) in cuvette experiments. The emission enhancement in PBS upon addition of 8 equivalents of CB7 was found to be 2.1-fold (Figure S15), with practically imperceptible changes in the fluorescence lifetime (4.8 and 4.6 ns in PBS and CB7, respectively). In fact, these lifetimes are practically identical to the ones measured for the free dye (Table 1).

We also tested the photostability of **DPP-COOH** and **DPP-COOH@CB7** in cells labeled with the nanobody (Figure S16). To this end, confocal images were repeated for 100 frames in the same corresponding regions of interest (ROIs, Figure S16A–B) and at the same excitation power used for the acquisition of other images (Figures 3–4). In principle, it appears that the free markers in PBS endure approximately twice as many frames (84 vs. 44), before half of the initial signal (average pixel intensity) has been bleached (Figure S16C–D). However, when considering the total signal (cumulative sum), the advantages of the formation of the supramolecular complex become evident. At its half-bleaching frame, the complex provided a 4-fold increase in the total signal (Figure S16E) compared to the free dye in PBS (without CB7). Likewise, it is necessary to accumulate 8 frames in PBS to obtain the same signal as with CB7 in one (first) frame (Figure S16F). Thus, despite the complexity of cellular environment and the fact that in confocal imaging the fluorophore is exposed to a much higher excitation intensity than in cuvette experiments, a better photo-fatigue resistance was also observed for DPP after treatment with CB7 in cells.

Encouraged by the strong fluorescence enhancement of DPP emission upon CB7 addition to nanobody-labeled cells, we imaged the stained cell by means of super-resolution STED microscopy. Based on the emission spectra (Figure 2a), we used two commercially available STED lasers for the depletion, 595 nm and 655 nm. As shown in Figure 5, STED microscopy with both lasers was possible, with optical resolution clearly beyond the diffraction limit. As two different microscopes were used, the excitation was performed with different lasers (485 nm and 518 nm respectively), and therefore slightly different detection windows were used. No undesired re-excitation produced by the STED laser was observed, even when a 595 nm STED laser was used. A direct comparison of STED imaging with and without CB7 (Figure S17) further demonstrates the advantages of our supramolecular complexation strategy.

Well-performing STED dyes with excitation and emission maxima similar to DPP (480 nm/550 nm, respectively) are scarce. The nearest spectral analog is the long Stokes shift dye Dyomics 485XL with its 485 nm/560 nm excitation/emission maxima in ethanol,[21] and it has been reported to excel in STED imaging with a 647 nm depletion laser.[22]

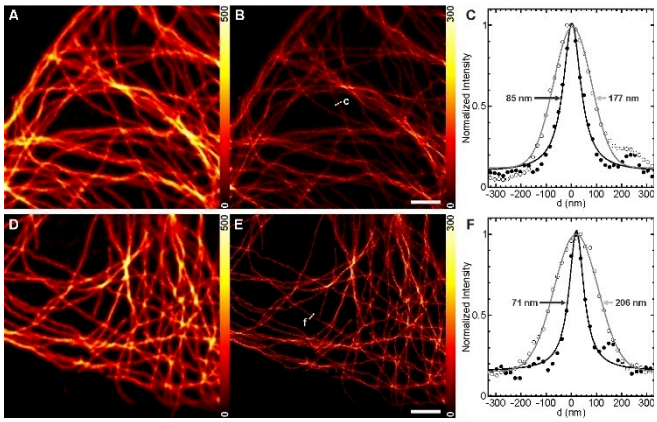

Figure 5. Confocal (A,D) and STED (B,E) images of U2OS cells stained with a primary antibody against tubulin and a secondary nanobody labeled with **DPP-COOH-Male** and mounted in PBS supplemented with CB7. STED was performed with a 655 nm laser (B) or with a 595 nm laser (E), both at approximately same power. (C,F) Confocal (empty symbols) and STED (filled symbols) line-profiles across a single filament from the indicated positions. Data was fit to a Gaussian function (Confocal) and a Lorentzian function (STED), with the corresponding FWHM indicated. Scale bars: 2 μm.

Therefore, we compared the performance of DPP and this benchmarked dye. For that, we took the same unlabeled nanobody and stained it with a maleimide derivative of Dyomics 485XL, also achieving quantitative labelling (Figure S12B). Then, cells were stained under very similar conditions: the same primary antibody, nanobody concentrations, etc. For Dyomics 485XL, the observed signal enhancement upon CB7 addition was only 4–12 % (~1.1-fold, Figure S18). The STED microscopy with this dye gave similar results as for DPP (Figure S19). The apparent sizes of single filaments were similar to the values reported in the literature,[22b] and slightly larger than the values obtained with **DPP**@CB7. In general, we found that DPP conjugates gave better images when used with a 595 nm STED laser, while DY-485XL was performing better with a 655 nm STED laser. Probably, a higher re-excitation produced by the 595 nm STED laser for DY-485XL, on the one hand, and the better fatigue resistance of this dye at higher STED laser powers (Figure S20), on the other hand, were the reasons for this difference. In fact, it was possible to increase the STED power to the maximum available for DY-485XL (Figure S19E), in order to improve the optical resolution, with still acceptable photobleaching (Figure S20).

We finally evaluated the applicability of the **DPP**@CB7 complex for two-color imaging in combination with a benchmark far-red emitting dye STAR635P. The rhodamine STAR635P was selected due to its absorption and emission maxima (638/651 nm), high brightness (90 % fluorescence quantum yield, $\varepsilon \sim 10^5\ M^{-1}\,cm^{-1}$),[23] photostability, and its excellent performance in STED microscopy with a 775 nm STED laser. As the complex **DPP**@CB7 has yellow fluorescence, the emission colors of the two components can be easily separated by using 485 nm and 640 nm excitation and proper detection ranges (see Figure 6A, 6C and the

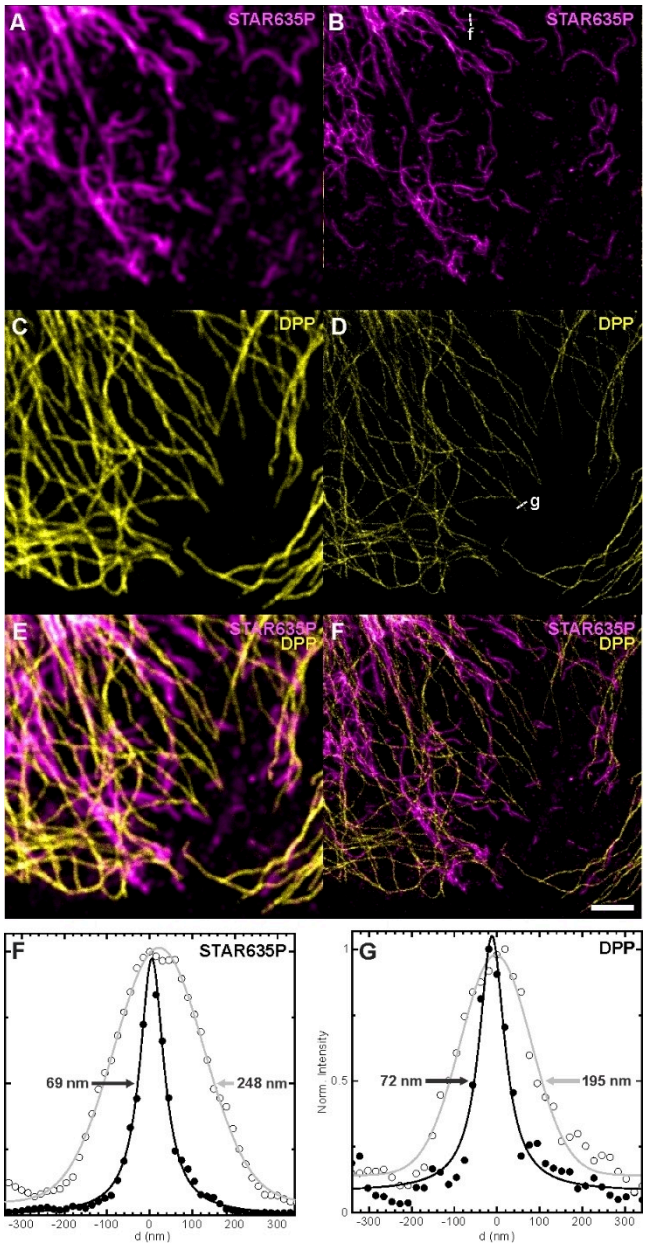

Figure 6. Two-color image of fixed U2OS cells stained with primary antibodies against tubulin (rabbit) and vimentin (mouse), a secondary nanobody (anti-rabbit) labelled with **DPP-COOH-Male** and a secondary antibody (anti-mouse) labelled with STAR635P. Color channels were imaged sequentially: first the red channel with 775 nm STED laser and then the green channel with 595 nm STED laser. Images were acquired after the addition of CB7. (A,B) Confocal and STED images recorded with 640 nm excitation and 650–763 nm detection; (C,D) Confocal and STED images recorded with 485 nm excitation and 510–585 nm detection; (E, F) Images for confocal and STED channels overlapped; (F,G) Confocal (empty symbols) and STED (filled symbols) line profiles across a single filament from the corresponding channels. Data were fit to a Gaussian function (Confocal) and a Lorentzian function (STED), with the corresponding FWHM indicated. Scale bar: 2 μm.

legend therein). The fluorescence lifetime and signal intensity of the far-red emitting dye STAR635P did not change upon CB7 addition (Figure S14C–D and S21A). Furthermore, two-color super-resolution STED imaging was demonstrated (Figure 6) by using a sequential process with the far-red STED channel recorded first, as the powerful 595 nm STED laser bleaches the red dye. This sequential imaging approach was necessary due to the low STED efficiency of DPP at 775 nm (Figure S22), preventing an imaging approach with a single STED laser. Other established and commercially available dyes with spectral properties similar to STAR635P (e.g., SiR—silicon rhodamine, and Alexa Fluor 647—a cyanine dye) can also be combined with **DPP**@CB7, (Figure S21B–C), accounting for the versatility of the **DPP**@CB7 complex in multi-color fluorescence imaging.

Conclusion

We prepared a supramolecular complex containing a diketopyrrolopyrrole fluorophore as a bright, photostable, long Stokes-shift dye for STED microscopy with depletion at yellow-red wavelengths (595–655 nm). Replacing the chlorine atoms in Ferrari Red core, we developed compounds with (trimethylammonio)phenyl groups having fairly good solubility in water, tightly binding with CB7 ligands, with the absorption and emission bands fitting commercially available laser lines for excitation and depletion, respectively. After studying the binding properties, and upon photophysical characterization, the imaging performance in far-field fluorescence microscopy was evaluated. The **DPP**@CB7 pair shows specific labelling of mitochondria in living cells, with enhanced cell-membrane permeability boosted by CB7 complexation. After decoration with carboxylic acid residues, the reactive forms of **DPP-COOH** were conjugated with secondary antibodies and nanobodies, affording specific labelling on fixed cells. The partial quenching of dye emission on proteins was overcome by addition of CB7. The protection offered by CB7 enhanced the emission, improved the fatigue resistance of the fluorophore, and allowed super-resolution imaging in a commercial STED microscope. We demonstrated a resolution enhancement, comparable to a bench-marked STED dye with large Stokes shift, but belonging to a distinct fluorophore class. We finally combined the new dye with the far-red emitting rhodamine and applied this pair in two-color STED microscopy with either 485 nm/595 nm, or 640 nm/775 nm excitation/depletion combination. The main challenge pertaining to future applications in life science, particularly in experiments with living cells, relates to the observation that large amounts of the CB7 host are necessary to overcome the competing effect of the cations present in aqueous buffers (despite the fact that in pure water binding is saturated with 2–4 equiv. of CB7). However, the CB7 concentration used in our live-cell experiments has been previously found to be non-toxic and well tolerated by cells. This study shows that the supramolecular nanosized complexes, based on fluorophores with optical properties enhanced by the host, are promising candidates for developing STED and other super-resolution techniques beyond their present limits.

Acknowledgements

D. K. acknowledges the Basic Science Research Program through the National Research Foundation of Korea (NRF) funded by the Ministry of Education (2021R1A6A3A03039133) and the Manfred Eigen fellowship program of MPI-NAT. The authors are grateful to J. Bienert, (Facility for Synthetic Chemistry, MPI-NAT), Dr. H. Frauendorf, the central analytics' team (Institute for Organic and Biomolecular Chemistry, Georg-August University, Göttingen) for acquiring NMR and ESI-MS spectra, to Prof. S. Jakobs (MPI-NAT) for providing the U2OS-Vim-Halo cell line. We thank A. Fischer (Optical Nanoscopy Department, MPI-MR) for help with cell culture and labelling, Dr. S. Fabritz and the staff of the MS core facility (MPI-MR), and Dr. E. D'Este and the staff of the Optical Microscopy Facility (MPI-MR). We are grateful to 2bind GmbH for performing the ITC measurements and analysis, in particular to Dr. Thomas Klein for his technical support. We thank Dr. Stephan Niebling (SPC facility at EMBL Hamburg) for performing the ITC measurements, analysis and discussion. Open Access funding enabled and organized by Projekt DEAL.

Conflict of Interest

The authors declare no conflict of interest.

Data Availability Statement

The data that support the findings of this study are available in the supplementary material of this article.

Keywords: Cucurbituril · Diketopyrrolopyrrole · Supramolecular Chemistry · Fluorescence · STED microscopy

[1] a) J. B. Grimm, A. N. Tkachuk, R. Patel, S. T. Hennigan, A. Gutu, P. Dong, V. Gandin, A. M. Osowski, K. L. Holland, Z. J. Liu, T. A. Brown, L. D. Lavis, *J. Am. Chem. Soc.* **2023**, *145*, 23000–23013; b) L. Wang, M. S. Frei, A. Salim, K. Johnsson, *J. Am. Chem. Soc.* **2019**, *141*, 2770–2781; c) S. J. Sahl, S. W. Hell, S. Jakobs, *Nat. Rev. Mol. Cell Biol.* **2017**, *18*, 685–701.

[2] for recent reviews, see: a) S. Zeng, X. Liu, Y. S. Kafuti, H. Kim, J. Wang, X. Peng, H. Li, J. Yoon, *Chem. Soc. Rev.* **2023**, *52*, 5607–5651; b) J. B. Grimm, L. D. Lavis, *Nat. Methods* **2022**, *19*, 149–158; c) L. D. Lavis, *Biochemistry* **2017**, *56*, 5165–5170.

[3] for recent reviews, see: a) G. Jacquemet, A. F. Carisey, H. Hamidi, R. Henriques, C. Leterrier, *J. Cell Sci.* **2020**, *133*, jcs240713. DOI: 10.1242/jcs.240713; b) K. Prakash, B. Diederich, R. Heintzmann, L. Schermelleh, *Phil. Trans. A Math. Phys. Eng. Sci.* **2022**, *380*, 20210110. DOI: 10.1098/rsta.2021.0110; c) S. Liu, P. Hoess, J. Ries, *Ann. Rev. Biophys.* **2022**, *51*, 301–326; d) J. Valli, A. Garcia-Burgos, L. M. Rooney, B. Vale de Melo e Oliveira, R. R. Duncan, C. Rickman, *J. Biol. Chem.* **2021**, *297*, 100791.

[4] a) R. N. Dsouza, U. Pischel, W. M. Nau, *Chem. Rev.* **2011**, *111*, 7941–7980; b) X. Ma, Y. Zhao, *Chem. Rev.* **2015**, *115*, 7794–7839; c) G. Hettiarachchi, D. Nguyen, J. Wu, D. Lucas, D. Ma, L. Isaacs, V. Briken, *PLoS One* **2010**, *5*, e10514, DOI: 10.1371/journal.pone.0010514; d) X. Zhang, X. Xu, S. Li, L.-H. Wang, J. Zhang, R. Wang, *Sci. Rep.* **2018**, *8*, 8819; e) T. A. Martyn, J. L. Moore, R. L. Halterman, W. T. Yip, *J. Am. Chem. Soc.* **2007**, *129*, 10338–10339; f) W. M. Nau, J. Mohanty, *Int. J. Photoenergy* **2005**, *7*, 133–141.

[5] J. Mohanty, W. M. Nau, *Angew. Chem. Int. Ed.* **2005**, *44*, 3750–3754; *Angew. Chem.* **2005**, *117*, 3816–3820.

[6] a) P. Jana, T. Mukherjee, R. Khurana, N. Barooah, V. Soppina, J. Mohanty, S. Kanvah, *J. Photochem. Photobiol. A* **2019**, *384*, 112062; b) Q. Yu, G. Zhang, Y.-N. Wang, H.-C. Hao, R. Sun, Y.-J. Xu, J.-F. Ge, *Dyes Pigm.* **2022**, *207*, 110693; c) X. Song, F. Liu, S. Sun, J. Wang, J. Cui, X. Peng, *RSC Adv.* **2014**, *4*, 9326–9329; d) P. Montes-Navajas, M. González-Béjar, J. C. Scaiano, H. Garcia, *Photochem. Photobiol. Sci.* **2009**, *8*, 1743–1747; e) X. Miao, Y. Li, I. Wyman, S. M. Y. Lee, D. H. Macartney, Y. Zheng, R. Wang, *MedChemComm* **2015**, *6*, 1370–1374.

[7] a) Z. Man, Z. Lv, Z. Xu, J. Yao, H. Fu, *Adv. Funct. Mater.* **2021**, *31*, 2106516, DOI: 10.1002/adfm.202106516; b) D. Kim, A. Aktalay, N. Jensen, K. Uno, M. L. Bossi, V. N. Belov, S. W. Hell, *J. Am. Chem. Soc.* **2022**, *144*, 14235–14247; even the trace impurities in commercial HPLC-quality water could give a lower binding affinity: c) M. A. Alnajjar, W. M. Nau, A. Hennig, *Org. Biomol. Chem.* **2021**, *19*, 8521–8529.

[8] a) S. Qu, H. Tian, *Chem. Commun.* **2012**, *48*, 3039–3051; b) V. A. S. Almodôvar, A. C. Tomé, *Molecules* **2021**, *26*, 4758, DOI: 10.3390/molecules26164758; c) M. Kaur, D. H. Choi, *Chem. Soc. Rev.* **2015**, *44*, 58–77.

[9] a) Q. Liu, S. E. Bottle, P. Sonar, *Adv. Mater.* **2020**, *32*, 1903882; b) W. Herbst, K. Hunger, *Industrial Organic Pigments, 3rd ed.*, VCH, Weinheim **2004**, pp. 487–490; c) W. Li, L. Wang, H. Tang, D. Cao, *Dyes Pigm.* **2019**, *162*, 934–950; for a recent review on chemistry of 2,5-dihydropyrrolo[3,4-c]pyrrole-1,4-diones, see: d) S. A. L. Shaikh, S. S. Birajdar, S. D. Ambore, A. L. Puyad, P. Vijayanand, S. V. Bhosale, S. V. Bhosale, *Results in Chem.* **2022**, *4*, 100473, DOI: 10.1016/j.rechem.2022.100473.

[10] a) S. J. Barrow, S. Kasera, M. J. Rowland, J. del Barrio, O. A. Scherman, *Chem. Rev.* **2015**, *115*, 12320–12406; for a recent report, see: b) K. Jelínková, A. Závodná, J. Kaleta, P. Janovský, F. Zatloukal, M. Nečas, Z. Prucková, L. Dastychová, M. Rouchal, R. Vícha, *J. Org. Chem.* **2023**, *88*, 15615–5625.

[11] R. Beninatto, G. Borsato, O. De Lucchi, F. Fabris, V. Lucchini, E. Zendri, *Dyes Pigm.* **2013**, *96*, 679–685.

[12] M. Pieczykolan, B. Sadowski, D. T. Gryko, *Angew. Chem. Int. Ed.* **2020**, *59*, 7528–7535; *Angew. Chem.* **2020**, *132*, 7598–7605.

[13] The origin of the large Stokes shifts of DPP dyes has been explained: a) T. Potrawa, H. Langhals, *Chem. Ber.* **1987**, *120*, 1075–1078; b) A. L. Koner, W. M. Nau, *Supramol. Chem.* **2007**, *19*, 55–66.

[14] a) Z. Li, S. Sun, Z. Yang, S. Zhang, H. Zhang, M. Hu, J. Cao, J. Wang, F. Liu, F. Song, J. Fan, X. Peng, *Biomaterials* **2013**, *34*, 6473–6481; b) M. M. Ayhan, E. Özcan, F. Alkan, M. Çetin, İ. Ün, D. Bardelang, B. Çosut, *Mater Adv* **2022**, *3*, 547–553; c) X. Miao, Y. Li, I. Wyman, S. M. Y. Lee, D. H. Macartney, Y. Zheng, R. Wang, *MedChemComm* **2015**, *6*, 1370–1374; d) F. Chandra, P. Kumar, A. L. Koner, *Colloids Surf. B* **2018**, *171*, 530–537.

[15] a) A. H. Shaib, A. A. Chouaib, R. Chowdhury, D. Mihaylov, C. Zhang, V. Imani, S. V. Georgiev, N. Mougios, M. Monga, S. Reshetniak, et al., DOI: 10.1101/2022.08.03.502284 (BioRxiv); b) S. J. Sahl, J. Matthias, K. Inamdar, T. A. Khan, M. Weber, S. Becker, C. Griesinger, J. Broichhagen, S. W. Hell, DOI: 10.1101/2023.07.07.548133 (BioRxiv).

[16] Á. Szabó, T. Szendi-Szatmári, L. Ujlaky-Nagy, I. Rádi, G. Vereb, J. Szöllősi, P. Nagy, *Biophys. J.* **2018**, *114*, 688–700.

[17] R. P. J. Nieuwenhuizen, M. Bates, A. Szymborska, K. A. Lidke, B. Rieger, S. Stallinga, *PLoS One* **2015**, *10*, e013907.
[18] H. Chen, S. S. Ahsan, M. B. Santiago-Berrios, H. D. Abruña, W. W. Webb, *J. Am. Chem. Soc.* **2010**, *132*, 7244–7245.
[19] L. A. Logsdon, C. L. Schardon, V. Ramalingam, S. K. Kwee, A. R. Urbach, *J. Am. Chem. Soc.* **2011**, *133*, 17087–17092.
[20] A. R. Urbach, V. Ramalingam, *Isr. J. Chem.* **2011**, *51*, 664–678.
[21] The data of manufacturer: https://dyomics.com/en/products/megastokes-dyes/dy-485xl.
[22] a) R. Schmidt, C. A. Wurm, S. Jakobs, J. Engelhardt, A. Egner, S. W. Hell, *Nat. Methods* **2008**, *5*, 539–544; b) C. Kempf, T. Staudt, P. Bingen, H. Horstmann, J. Engelhardt, S. W. Hell, T. Kuner, *PLoS One* **2013**, *8*, e62893; c) C. Dean, H. Liu, T. Staudt, M. A. Stahlberg, S. Vingill, J. Bückers, D. Kamin, J. Engelhardt, M. B. Jackson, S. W. Hell, E. R. Chapman, *J. Neurosci.* **2012**, *32*, 5398–5413.
[23] The data of the manufacturer: https://abberior.shop/abberior-STAR-635P.

Manuscript received: May 30, 2024
Accepted manuscript online: June 17, 2024
Version of record online: August 2, 2024